Lasers in Surgery and Medicine 26:421–434 (1999)

Comparison of Cortical Bone Ablations by Using Infrared Laser Wavelengths 2.9 to 9.2 μm

George M. Peavy, DVM,[1]* Lou Reinisch, PhD,[2] John T. Payne, DVM,[3] and Vasan Venugopalan, ScD[1,4]

[1]*Beckman Laser Institute and Medical Clinic, College of Medicine, University of California, Irvine, California*
[2]*Department of Otolaryngology, Vanderbilt University Medical Center, Nashville, Tennessee*
[3]*Department of Small Animal Surgery, University of Missouri-Columbia, College of Veterinary Medicine, Columbia, Missouri*
[4]*Department of Chemical and Biochemical Engineering and Materials Science, University of California, Irvine, California*

Background and Objective: **The purpose of this study was to compare the ablation of cortical bone at wavelengths across the near and midinfrared region.**
Study Design/Materials and Methods: **An free electron laser generating 4-μs macropulses at specific wavelengths between 2.9 and 9.2 μm was used to ablate cortical bone. The same pulse intensity, repetition rate, radiant exposure, number of pulses, and delivery was used for each wavelength. Tissue removal, collateral thermal injury, and morphologic characteristics of the ablation sites were measured by light and scanning electron microscopy, and compared with the infrared absorption characteristics of cortical bone.**
Results: **Within the parameters used, bone ablation was found to be wavelength dependent. Incisions were deepest where protein has strong absorption, and were most shallow where mineral is a strong absorber. No char was observed on ablation surfaces where 3.0, and 5.9–6.45 μm wavelengths were used.**
Conclusions: **The use of wavelengths in the 6.1-μm amide I to 6.45-μm amide II region, with the pulse characteristics described, were the most efficient for cutting cortical bone and produced less collateral thermal injury than cutting with a surgical bone saw. This study confirms previous observations that the ablation mechanism below plasma threshold is consistent with an explosive process driven by internal vaporization of water in a confined space and demonstrates that ablation is enhanced by using wavelengths that target the protein matrix of cortical bone. Lasers Surg. Med. 25:421–434, 1999.** **© 1999 Wiley-Liss, Inc.**

Key words: free electron laser, laser osteotomy, laser bone cutting, orthopedics

Contract grant sponsor: Department of the Navy, Office of Naval Research; Contract grant number: N00014-94-0874; Contract grant sponsor: Laser Microbeam and Medical Program (LAMMP), an NIH Biotechnology Resource; Contract grant number: RR-01192; Contract grant sponsor: Beckman Laser Institute and Medical Clinic, University of California, Irvine; Contract grant sponsor: W.M. Keck Free-Electron Laser Center, Vanderbilt University.

The content of this manuscript does not necessarily reflect the position of the Government, and no official endorsement should be inferred.

Dr. Payne's current address is: Veterinary Surgical Service, Tennessee Avenue Animal Hospital, 1381 Tennessee Avenue, Cincinnati, OH 45229.

*Correspondence to: George M. Peavy, DVM, Beckman Laser Institute and Medical Clinic, University of California, Irvine, CA 92612.

Accepted 15 June 1999

INTRODUCTION

The cutting of bone is a common procedure in orthopedic surgery, used to access structures protected by bony surfaces, correct or reconstruct skeletal abnormalities, attach orthopedic appliances, and allow the implantation of joint prostheses. Failure to perform an accurate osteotomy may result in injury to surrounding tissue or organs or contribute to either reconstruction or implant failure. Osteotomy precision is often diminished by the limitations imposed by the use of a hand-held pneumatic osteotomy saw. Use of a laser to incise bone could permit more controlled cutting, especially if coupled with a computer or robotic control device.

Conventional lasers allow the use of a single wavelength or harmonics of that wavelength for clinical application; however, the free electron laser (FEL) allows the selection of wavelengths across a broad spectrum in the infrared (IR) range. The Vanderbilt FEL can be used to produce wavelengths between 2.8 and 9.3 μm, in 4.0-microsecond (μs) macropulses, which are composed of a series of 1- to 2-picosecond (ps) micropulses delivered 350 ps apart. The versatility of the FEL allows for the selection and comparison of laser wavelengths across the near and mid-IR ranges while maintaining the same energy and pulse structure.

Characteristics of bone ablation have been reported for the specific wavelengths and modes of the Eximer, Ho:YAG, HF, Er:YAG, and CO_2 lasers [1–23]. Studies that use near to mid-IR wavelengths to compare ablations of various hard tissues by different laser systems have demonstrated dependence on both wavelength and pulse duration. The wavelength dependence has been attributed to the spectral absorption properties of the tissue water and mineral components [6,12, 15,16,24,25].

In a previous study, we determined that in vivo specimens of cortical bone can be ablated at 3.0-, 6.1-, and 6.45-μm wavelengths, by using the pulse structure described here, with minimal alterations in the chemical composition of the ablation surface as determined by Fourier transform infrared (FTIR) photoacoustic spectrometry (PAS) [26]. The purpose of this study is to determine whether bone ablation exhibits a wavelength dependence across the IR region when the pulse characteristics of the incident irradiation are maintained the same for each ablation. Specifically, we wanted to examine the relationship between the observed characteristics of laser cuts to the IR absorption spectrum of cortical bone, with the aim of determining whether cut depth could be enhanced by wavelength selection while inducing less collateral tissue injury than that produced by a conventional surgical bone saw.

MATERIALS AND METHODS

A FEL was used to produce wavelengths between 2.9 and 9.2 μm, delivered in 4.0-μs macropulses composed of a series of 1- to 2-ps micropulses, delivered 350 ps apart. The macropulse repetition rate was 30 Hz, pulse energy was 22.5 ± 2.5 mJ/pulse, and the beam was directed through a 200-mm focal length calcium fluoride or barium fluoride lens into a 200-μm diameter spot. The wavelength composition of the FEL beam is approximately ±0.5% of the wavelength at full width half-maximal height.

Before performing ablations at each wavelength, the focal distance for the selected lens was determined for the specific wavelength by collecting serial ablations at varying focal distances. The distance between the lens and the surface of each specimen was adjusted to conform to the focal distance established for each wavelength. The spot size was again confirmed by obtaining four individual ablation spots on a wooden tongue depressor placed at the focal distance determined for the wavelength and measuring the crater diameter under magnification.

A previously described computer controlled delivery system [27] was used to direct the beam along the ablation surface. Each successive macropulse was directed in a rotating order to one of five equal length segments of the programmed ablation line. After delivery of the fifth macropulse, the order was repeated; however, the beam was offset from the previous ablation spot of each segment by 10% of the spot diameter. Each 6.6-mm ablation line consisted of three complete 11-second passes of 328 individual overlapping macropulses with the accumulated total of 10 pulses delivered per spot diameter per pass. Radiant exposure delivered along the ablation line was 716 J/cm2 per pass, for a total of 2,150 J/cm2 delivered for the complete ablation.

Fresh bovine cadaver femur specimens were collected from a slaughterhouse. The mid-shaft portions were isolated and sectioned into approximately 3 × 4 cm blocks of cortical bone by using a commercial band saw. The specimens were placed on normal saline-soaked cotton cloth towels,

sealed in a plastic container, and refrigerated until used.

The specimens were used within 48 hours of collection. Individual specimens were selected at the time of use for presentation of a flat surface that would accommodate two to four ablation test sites. The periosteum was stripped from the surface. The sample was then wrapped in a normal saline-soaked gauze sponge and kept in a closed container before and after the ablation procedure.

Each specimen was placed on a fixed surface under the beam path and held in position with modeling clay. The focusing lens was adjusted to the appropriate distance to produce a 200-μm spot as previously determined for each wavelength. Gauze sponges soaked in normal saline were used to cover all portions of the bone specimen not being ablated.

A nitrogen-driven microsagittal bone saw (Micro 100 sagittal saw, no. 5053-11, Linvatec [Hall Surgical], Largo, FL) was used to make cuts in specimens that approximated the dimensions of the laser ablation cuts. Control bone specimen blocks of similar dimensions but without laser or bone saw ablations were selected and fixed at 0, 24, and 48 hours after collection. After the collection of all ablation specimens for each parameter, the excess bone was trimmed from each block and the blocks were then placed in sealed containers of 10% formalin and refrigerated.

Individual specimens were examined and imaged at 1.5 to 15× under a dissecting microscope (model SZH, Olympus Optical Co., LTD., Tokyo, Japan), rinsed and stored in phosphate buffer under refrigeration. Specimens for light microscopy were decalcified (Rapid Bone decalcifier, APEX Engineering Products Corporation, Plainfield, IL), dehydrated in progressive concentrations of ethanol, cleared (Histoclear, National Diagnostics, Manville, NJ), and infiltrated with paraffin in a tissue processor (model 166MP, Fisher Scientific, Pittsburgh, PA). The samples were then embedded in paraffin, cut in 6-μm-thick serial sections, mounted on glass slides, and stained with hematoxylin and eosin.

A minimum of 35 individual sections were prepared in series from the center portion of each ablation line specimen. The serial tissue sections were examined by light microscopy (model BH-2, Olympus Optical Co., LTD., Tokyo, Japan), and the section of each series with the deepest laser cut was used for evaluation. A specimen section for evaluation was selected from each of four different cuts for each wavelength ($n = 4$).

Light microscopy images were captured (Video Player software, Apple Computer Inc., Cupertino, CA) at 10× and 100× magnification by using a CCD camera (model DXC-101, Sony, Japan) attached to the microscope. The ablation sites were examined for cut depth, cross-sectional area, collateral thermal injury, presence of char, and morphologic characteristics. Measurement of tissue structures was performed digitally on a computer system (Power Mac G3, Apple Computer, Inc., Cupertino, CA) that used analytical software (IP Lab Spectrum 10, Signal Analytics Corp., Vienna, VA). A 2-mm micrometer standard was imaged and used to convert the measurement of pixels to distance in microns (8.333 μm per pixel at 10× and 0.83 μm per pixel at 100×).

RESULTS

Gross examination of the ablation specimens under a dissecting microscope revealed clean ablation surfaces free of char at wavelengths 2.9, 3.0, and 5.9–6.45 μm. For wavelengths 3.1–4.2, 5.0, and 6.6–7.5 μm, occasional areas of char were observed on one end of the ablation line but not along the walls. Only rare, slight char was noted on the lip of the ablations at 5.8, 8.0, 9.0, and 9.2 μm wavelengths (Fig. 1). In almost all cases where char was observed, it was confined to either the lip of the ablation edge or one end of an ablation line.

The ablation characteristics at each wavelength are presented in Figure 2 and Table 1. The most shallow laser cuts, which ranged from 0.95 to 1.08 mm deep, are observed with the wavelengths of 5.8, and 8.9–9.2 μm. An increase in cut depth is observed from 1.39 mm at the 2.9-μm wavelength to 1.73 mm at the 3.0-μm wavelength, although the cross sectional areas of each cut remain similar. Cut depth decreases for wavelengths 3.1 and 3.2 μm, increases again for the 4.2- and 5.0-μm wavelengths, then drops to 1.01 mm at the 5.8-μm wavelength. There is a progressive increase in cut depth from 1.01 mm to 2.55 mm between wavelengths 5.8 and 6.1 μm. Maximal cut depth is observed to be 2.55 mm at the 6.1 μm wavelength, drops slightly, approximating 2.31 mm through the 6.45 μm wavelength, then ranges between 1.74 mm and 1.93 mm with the wavelengths of 6.6 to 7.2 μm and again at 8.0 μm.

In Figure 3, the cut depth and cross-sectional area are plotted for each wavelength and compared with the previously reported infrared photoacoustic absorption spectrum for rabbit cortical

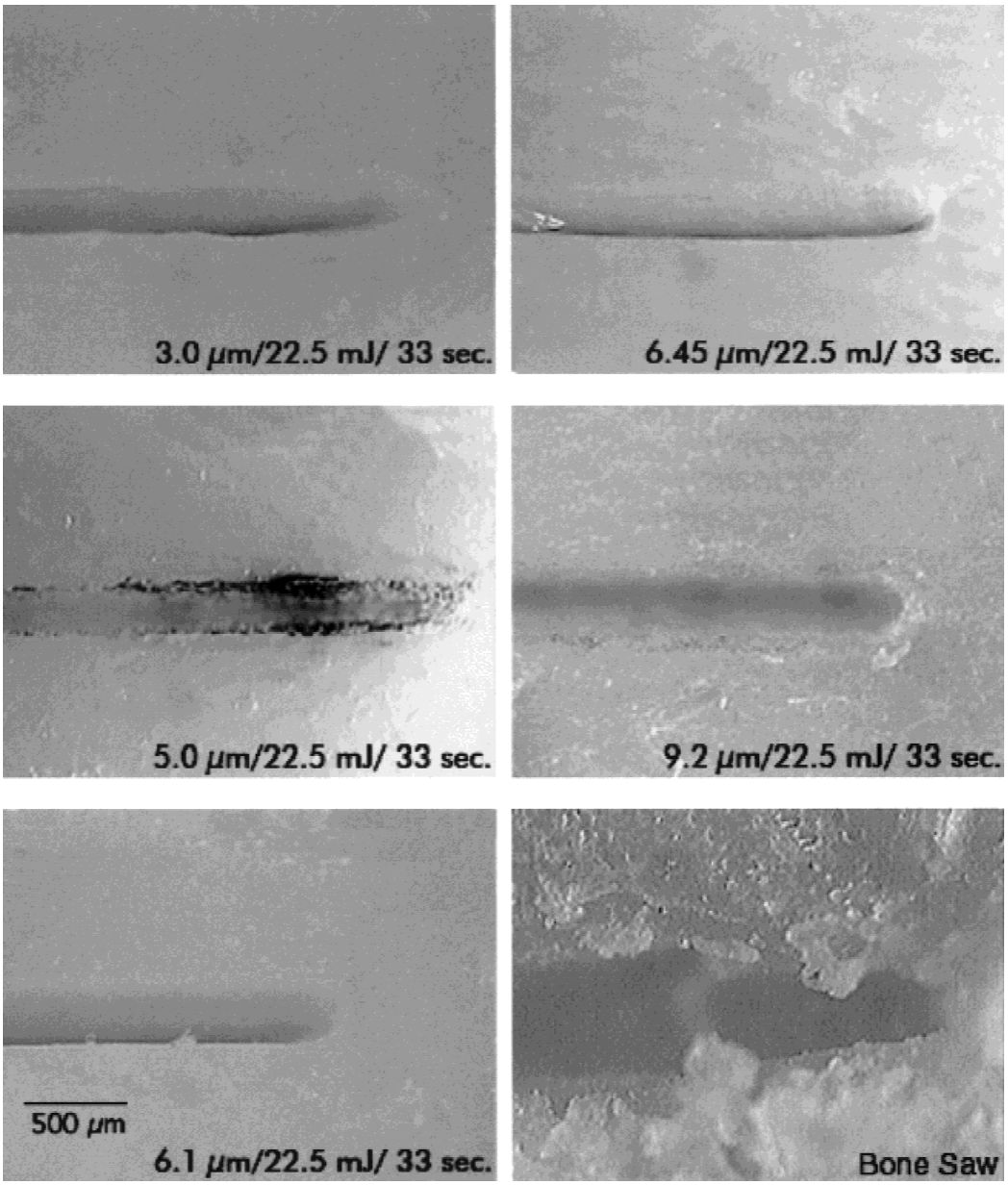

Fig. 1. Osteotomy cuts of cortical bone made by using a bone saw and FEL wavelengths 3.0, 5.0, 6.1, 6.45 and 9.2 μm, viewed under a dissecting microscope (original magnification, 15×. Clean cuts without evidence of any char were observed at 2.9-, 3.0-, and 5.9- to 6.45-μm wavelengths. As demonstrated by the view of the ablation at 5.0 μm, occasional areas of char were observed at one end or surface lip of some of the cuts made by using wavelengths 3.1–4.2, 5.0, 5.8, 6.6–7.5, 8.0, 9.0, and 9.2 μm. Bone saw cuts tend to be wider and have more particulate debris associated with them.

bone [26]. Cut depth seems to be related to the IR absorption spectrum in the regions of wavelengths 2.9–3.2 μm and between 5.8 and 8.0 μm, but is inversely related to absorption between 8.9 and 9.2 μm. Cut depth for wavelengths 4.2 and 5.0 μm does not seem to correlate with the IR absorption spectrum and relative cut depths observed for the other wavelengths.

Collateral thermal injury, as measured from the crater wall at the midpoint of the crater depth along a line perpendicular to the side of the crater, is listed in Table 1. For most wavelengths the zone of collateral thermal injury ranges between 10 and 20 μm; however, it approximates 20–25 μm for wavelengths 2.9, 5.8, and 9.2 μm and is observed to be 30–35 μm for wavelengths 3.0, 4.2,

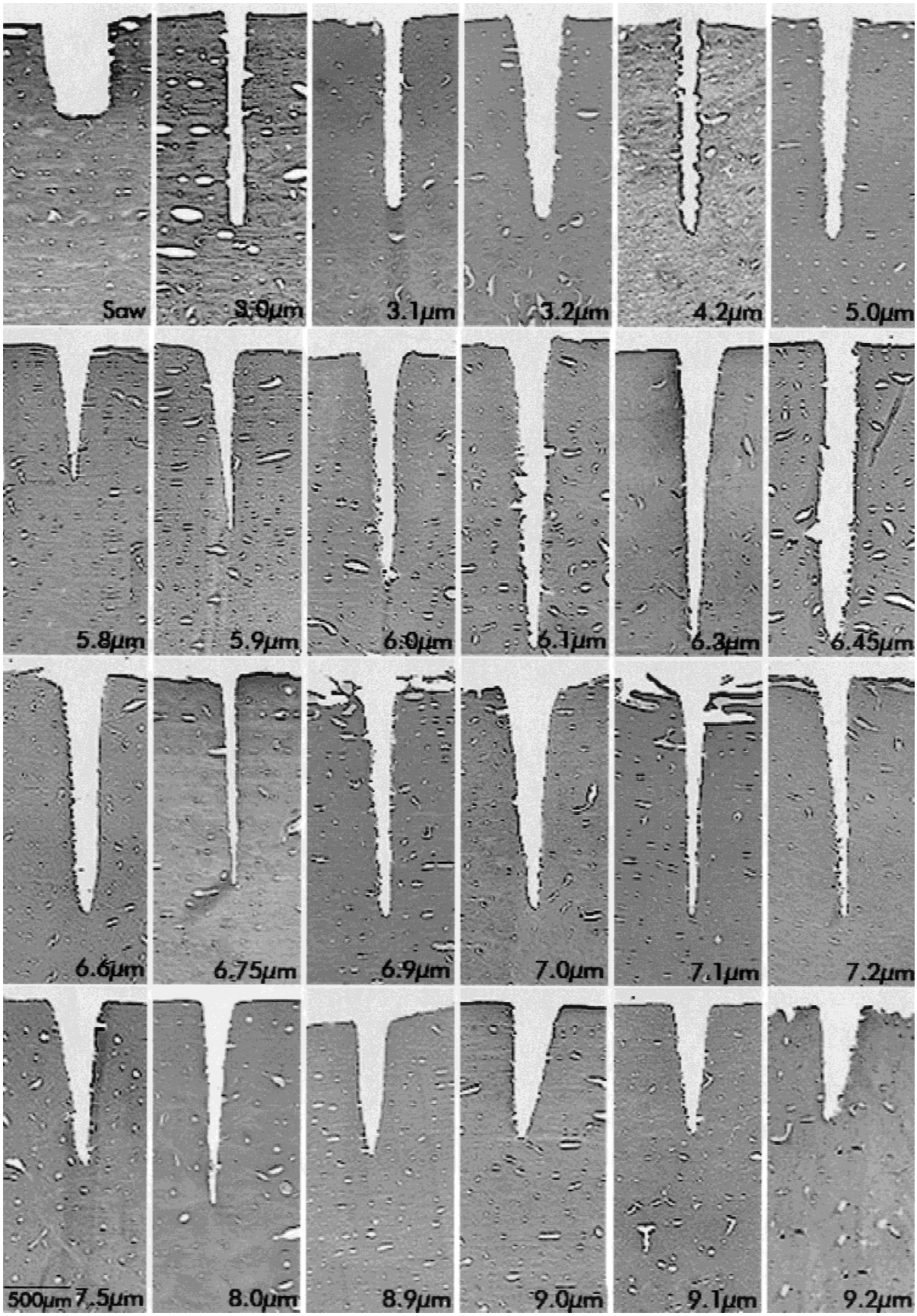

Fig. 2. Histology sections of bone saw cut and laser cuts of cortical bone made by using FEL wavelengths 2.9–9.2 μm, 200-μm spot size, and the equivalent of 30 individual macropulses with a total of 2,150 J/cm^2 delivered for each ablation. Cut depth is clearly wavelength dependent, with the deepest cuts occurring with wavelengths 6.1–6.45 μm, and the shallowest occurring for wavelengths 5.8 and 8.9–9.2 μm.

TABLE 1. Characteristics of Bovine Cortical Bone Cuts Made Using Laser Wavelengths 2.9 to 9.2 μm or a Sagittal Bone Saw*

λ (nm)	†μ_a water (mm^{-1})	††μ_a collagen (mm^{-1})	Cut depth (mm)		Cut cross-sectional area (mm^2)		Collateral thermal injury (μm)	
			Mean	±SD	Mean	±SD	Mean	±SD
2.9	1161	122	1.39	0.18	0.35	0.09	22.4	5.4
3.0	1139	237	1.73	0.31	0.32	0.06	29.2	12.1
3.1	778	126	1.51	0.02	0.31	0.12	12.1	0.6
3.2	363	81	1.56	0.08	0.51	0.06	15.7	3.5
4.2	21	8	1.62	0.10	0.33	0.08	34.1	8.7
5.0	31	7	1.79	0.08	0.31	0.10	29.8	11.2
5.8	72	30	1.01	0.09	0.16	0.02	23.1	10.9
5.9	132	160	1.38	0.13	0.21	0.03	16.3	5.2
6.0	224	664	1.96	0.82	0.36	0.05	10.2	4.6
6.1	270	848	2.55	0.06	0.41	0.05	15.1	0.8
6.3	114	99	2.34	0.89	0.43	0.05	13.8	1.9
6.45	82	362	2.31	0.12	0.56	0.08	17.8	3.0
6.6	68	218	1.91	0.36	0.41	0.10	19.1	3.5
6.75	62	69	1.93	0.22	0.27	0.09	18.0	2.5
6.9	59	108	1.76	0.18	0.28	0.02	12.0	6.0
7.0	57	82	1.74	0.48	0.33	0.09	17.3	3.6
7.1	57	95	1.84	0.85	0.26	0.11	11.7	1.4
7.2	56	77	1.86	0.10	0.22	0.11	7.4	5.5
7.5	55	59	1.51	0.21	0.27	0.02	7.1	1.0
8.0	54	110	1.73	0.12	0.25	0.07	12.0	3.1
8.9	55	39	1.05	0.09	0.21	0.03	15.1	2.5
9.0	56	48	1.08	0.64	0.20	0.04	12.8	3.2
9.1	57	48	1.08	0.07	0.22	0.02	10.8	8.1
9.2	57	50	0.95	0.04	0.20	0.04	23.0	9.0
Saw			0.83	0.20	0.42	0.22	23.4	13.6

*All laser cuts were made using a 4.0-μs macropulse, 200-μm spot diameter, pulse intensity of 72 J/cm^2, and total energy of 2,150 J/cm^2 for the cut. The width of the zone of collateral thermal injury was measured from the wall of the cut at the midpoint of the cut depth, along a line drawn perpendicular to the wall. Absorption coeficients (μ_a) were extrapolated from data previously reported for †water [35], and ††type I collagen [37]. For each parameter, n = 4.

and 5.0 μm. Collateral thermal injury on the sides of the bone saw cut vary greatly between specimens, with an observed range of 8.1–43.6 μm.

The area immediately adjacent to the ablation crater and bone saw cuts was subjectively evaluated for the presence and absence of cells within individual lacuna, and compared with similar areas at the same depth from the surface of the specimen but well away from the ablation area. Although there seems to be some decrease in the number of lacuna that contain cells immediately adjacent to all ablation sites, no distinct zone of empty lacuna could be identified for any of the specimens examined. In all cases, populated lacunae are found even within the area of collateral thermal injury. There is no difference in the relative number of populated and unpopulated lacunae observed in the laser cut specimens and the bone saw specimens.

SEM examination of the crater walls (Figs. 4–6) revealed a uniform surface of collagen tufts with varying degrees of melting, occasional intact crystals protruding from or resting on the surface, and no evidence of microfissures. The exposed collagen tufts on the surface of the laser ablations display a more roughened appearance on the bottom of the crater and a smoother texture along the wall moving toward the top of the crater. The size of the crystals observed on the surface of some samples are approximately 10 μm wide and range from 20 to over 50 μm in length. The surfaces of the bone saw cuts are very smooth in texture but broken into slabs by multiple microfissures.

DISCUSSION

Cortical bone is composed of an organic matrix (25–30% by weight), crystalline minerals (60–65%), and water (10%) [28]. The organic matrix is 90–95% type I collagen, and much of the rest is an amorphous ground substance. The collagen forms fibrils of individual 280-nm-long molecules that overlap neighboring molecules by 70 nm, with a space of 40 nm separating the ends of successive

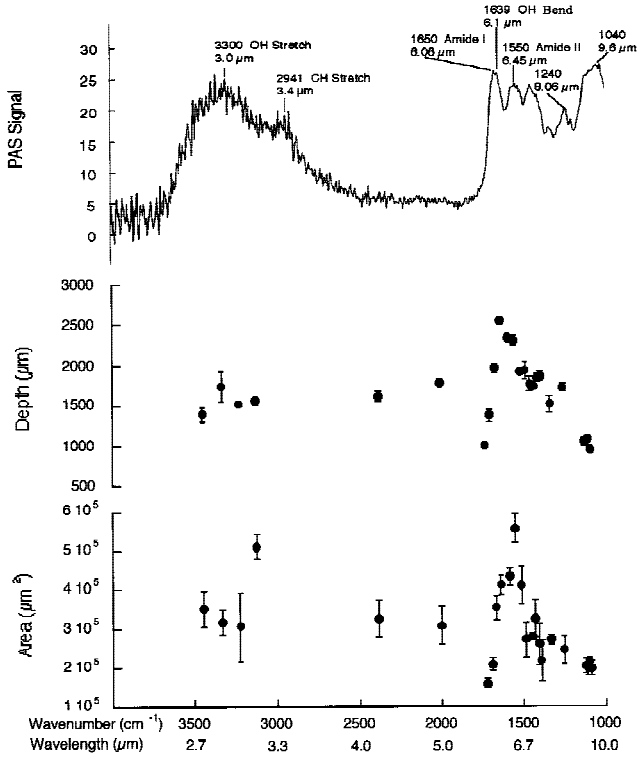

Fig. 3. Cut depth and area of bovine cortical bone laser ablations made by using FEL wavelengths 2.9–9.2 μm compared with the FTIR-PAS absorption characteristics of rabbit cortical bone similar to that previously reported [26]. The magnitude of the laser ablation cuts parallel the absorption characteristics of cortical bone for wavelengths 2.9–3.2 μm and 5.8–8.0 μm but are inversely proportional to the absorption characteristics for wavelengths 4.2, 5.0, and 8.9–9.2 μm. (FTIR-PAS courtesy of Dr. Paulette Spencer, School of Dentistry, University of Missouri, Kansas City).

molecules. The mineral component is predominantly calcium and phosphate apatite formed as needles, plates, or leaves which are distributed regularly along the collagen molecules, with as much as 50% of the total mineral deposited in the major 40-nm spacings. The amorphous cement substance, which contains proteoglycans, other proteins, and water, surrounds the apatite crystals and the collagen fibers. Collagen provides the structural framework of bone, whereas the mineral component adds strength and rigidity [28–32].

Bone apatite is characterized as a carbonate containing, poorly crystallized analog of the naturally occurring mineral hydroxyapatite, $Ca_{10}(PO_4)_6OH_2$. Bone mineral is distinct from geologic apatite because of its small crystallite size (40–50 nm × 25–35 nm, × 2.5–5.0 nm) and its structural imperfections [33]. Bone apatite is often modified by substitution of fluoride or chloride ions for hydroxyl groups and carbonate ions for the tetrahedral phosphate groups. Because the exact stoichiometry of bone mineral is dependent on age, isomorphous substitution, and other factors, it has been suggested that bone apatite should be described as a calcium-and-hydroxyl–deficient, hydrogen-and-carbonate–containing analog of hydroxyapatite that is characterized by structural imperfection and a high surface area [34].

Water has good optical absorption across the IR spectrum investigated in this study, with absorption peaks at 3.0 μm (O-H stretch) and 6.1μm (O-H bend) [35]. Absorption peaks attributable to protein are found at 3.0 μm (amide A), 3.25 μm (amide B), 6.06 μm (amide I), 6.45 μm (amide II), and 8.06 μm (amide III) [36]. The absorption coefficients (μa) for water [35] and collagen [37] are extrapolated from previously published data and are presented in conjunction with the observed ablation characteristics of cortical bone for each wavelength in this study (Table 1).

Although nonapatitic mono-, di-, and tribasic forms of calcium phosphate have moderate-to-strong absorption at wavelengths 3.1, 3.3, 4.3, 4.4, 6.07, 6.1, 8.1, 8.9–11.1 μm, calcium hydroxyapatite has only a moderate absorption peak at 2.81 μm and a strong absorption band from 8.9–11.1 μm [38–42]. Studies of rabbit cortical bone by FTIR-PAS have demonstrated the relative absorbance of wavelengths across the near to mid-IR spectrum [26] and a similar FTIR-PAS spectral analysis is presented in Figure 3. The calcium hydroxyapatite absorption at 2.81 μm seems to be masked by water absorption but predominates at wavelengths 8.9–11.1 μm.

The IR absorption spectrum observed for cortical bone is consistent with the combined absorption characteristics of water, collagen, and the calcium hydroxyapatites. Tissue removal by each of the wavelengths selected for this study were compared with each other, the IR absorption characteristics of bone (Fig. 3), and to the optical absorption of each of the components of bone. In this study, a single radiant exposure was used for each wavelength; therefore, we are not able to evaluate the variation of threshold exposure needed for material removal or the heat of ablation for each wavelength.

For the radiant exposure tested, results show wavelength dependence of the ablation process, with the deepest cuts observed between the wavelengths of 6.1 to 6.45 μm where water and

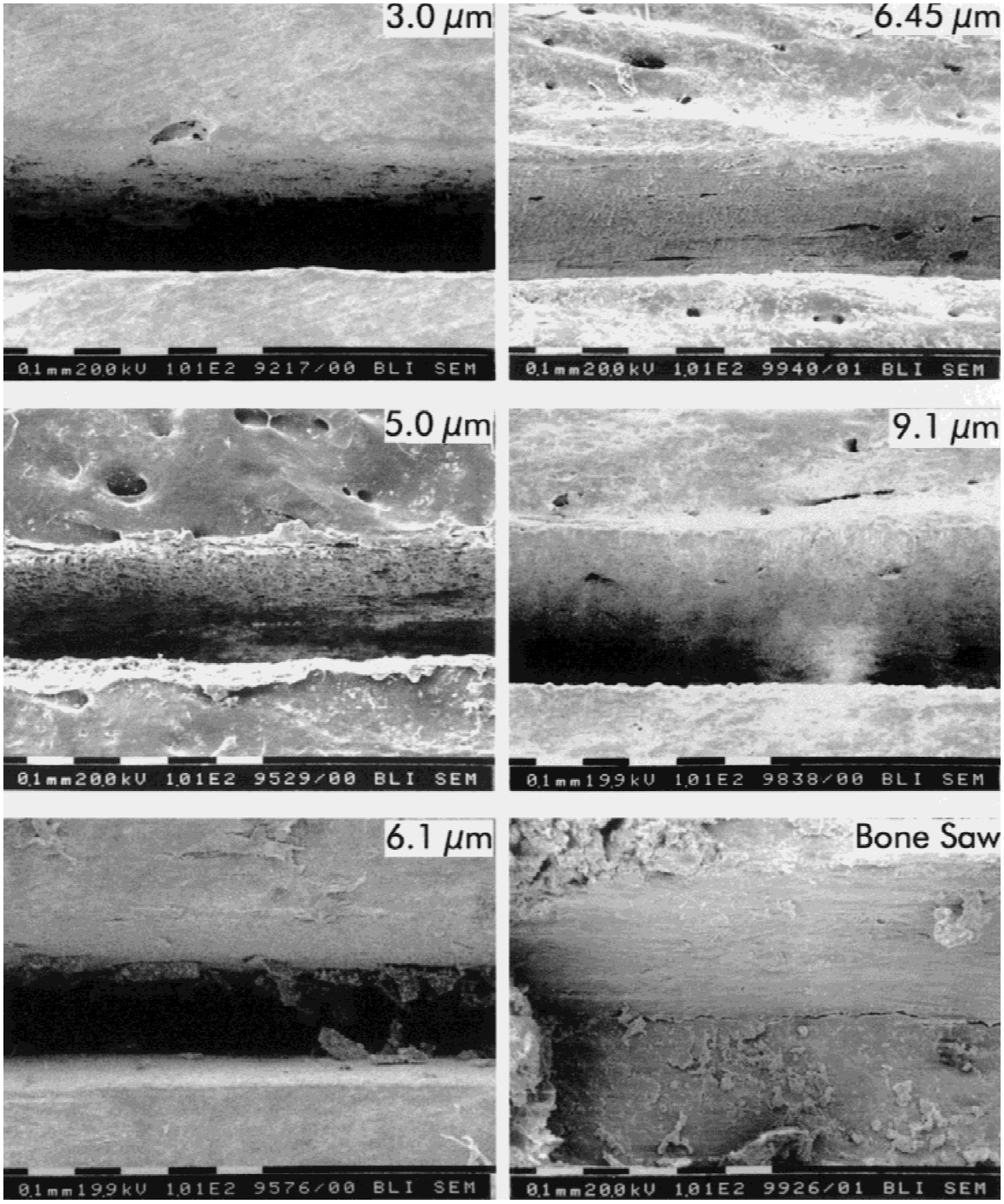

Fig. 4. Scanning electron photomicrograph (original magnification, 100×) view of cortical bone osteotomy sites demonstrates the clean, precise cuts of the laser, accumulation of mineral crystals on some laser ablation surfaces, and the large amount of accumulated debris at the bone saw cut site.

protein are especially good absorbers. Cut depth is less at the 3.0-μm wavelength where water is an especially good absorber, but absorption by protein is lower. With the exception of the 5.8-μm wavelength, the least amount of tissue was removed with wavelengths 8.9–9.2 μm where absorption by the hydroxyapatites predominate. This finding indicates that crater depth does not correlate with the combined absorption properties of the components of cortical bone.

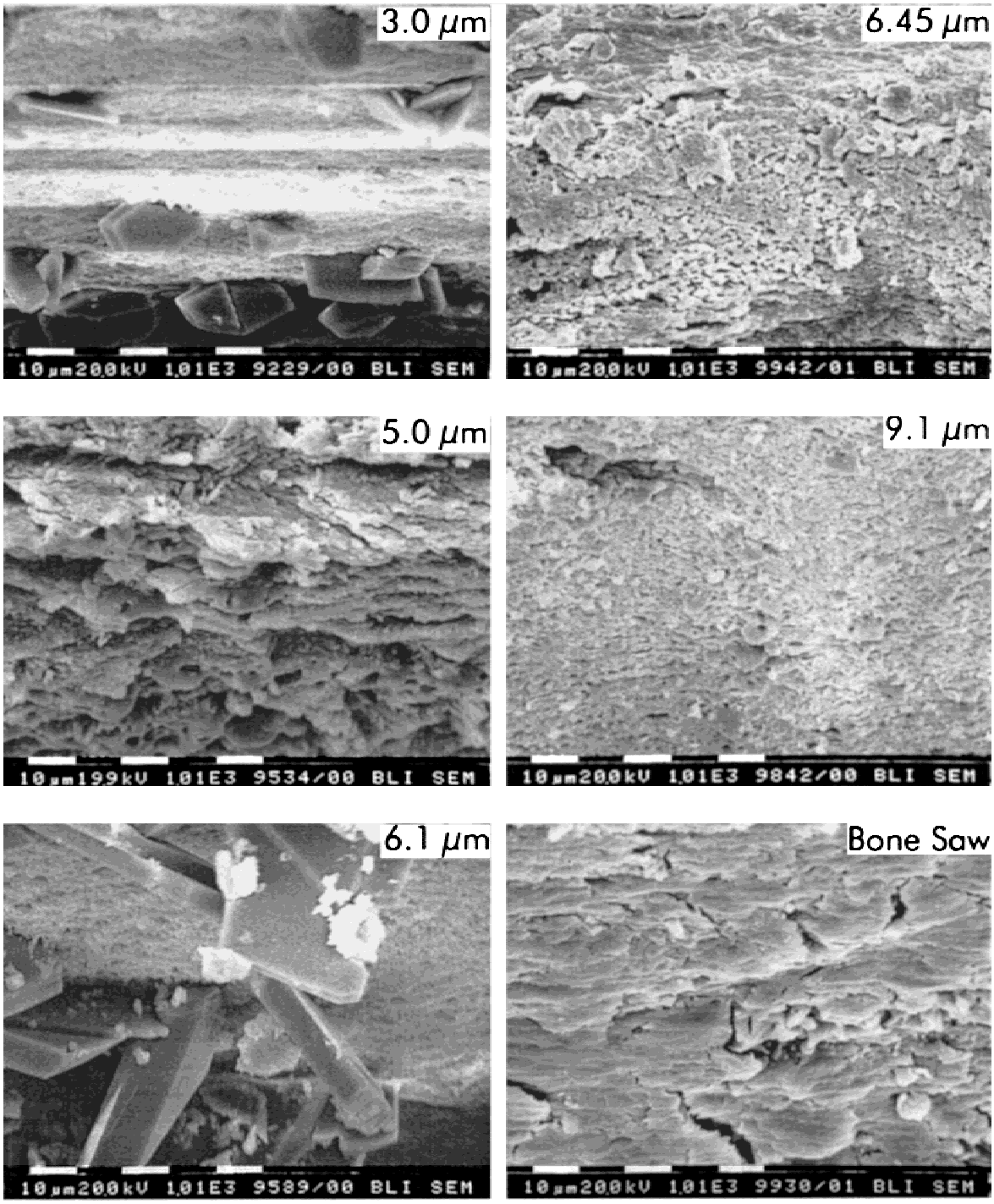

Fig. 5. Scanning electron photomicrograph (original magnification, 1,000×) views of the walls of laser osteotomy sites demonstrate a uniform surface of collagen tufts with varying degrees of melting, occasional intact crystals protruding from or resting on the surface, and no evidence of microfissures. The size of the crystals observed on the surface of some samples were approximately 10 μm wide and ranged from 20 to greater than 50 μm in length. The surface of the bone saw cut demonstrates the smooth texture broken into slabs by multiple microfissures.

The cut depth in cortical bone vs. the optical penetration depth of collagen (1/μa) for each wavelength tested was plotted (Fig. 7). Except for two outlying points corresponding to wavelengths 4.2 and 5.0 μm, there is excellent correlation between the depth achieved and the optical penetration depth of collagen. The relationship between cut depth and the optical absorption of water and

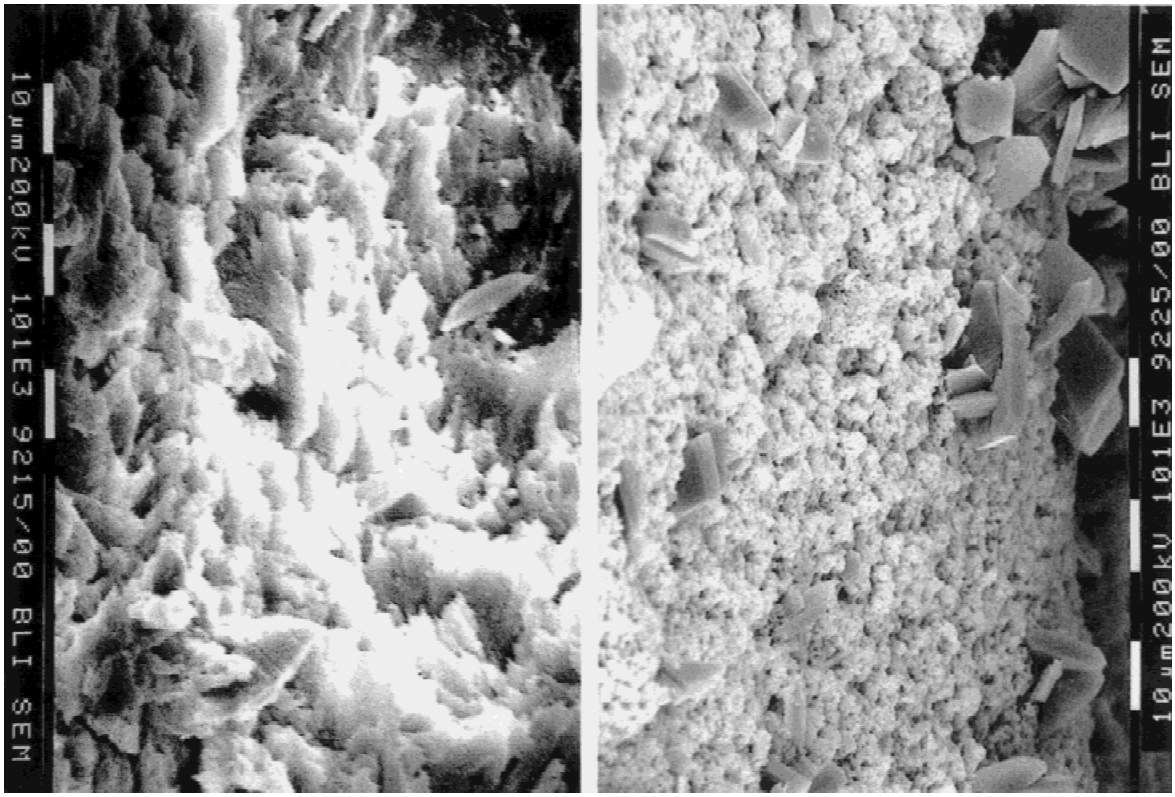

Fig. 6. Scanning electron photomicrograph (original magnification, 1,000×) view of cortical bone ablation by using FEL wavelength 3.0 μm. The exposed collagen tufts on the surface of laser ablations display a more roughened appearance on the bottom of the crater (left) and a smoother texture along the wall toward the top of the crater (right).

of calcium hydroxyapatite were examined and no correlation was found. To a first approximation, it appears that the degree of absorption by collagen, the primary structural component of bone, is the key determinant to the depth of cut. This finding is consistent with soft-tissue studies for which increased material removal has been demonstrated where laser wavelengths that target the structural matrix of the tissue are used [43,44].

The observations of cut depth at the 4.2-, 5.0-, and 5.8-μm wavelengths are not explained by this study, and require additional investigation. The observations at 4.2- and 5.0-μm wavelengths demonstrate that ablation of bone can be achieved where collagen, water, and calcium hydroxyapatite have poor optical absorption; however, a greater degree of collateral injury is observed.

For all of the wavelengths evaluated, collateral thermal injury of the laser ablation specimens was equal to or less than that observed for the bone saw. In almost all cases, the collateral thermal change was limited to a zone of 10–20 μm. Only at the wavelengths of 2.9, 3.0, 4.2, 5.0, 5.8, and 9.2 μm did the collateral thermal injury exceed 20 μm, and then only the 3.0-, 4.2-, and 5.0-μm wavelengths produced thermal injury that approached 30 μm.

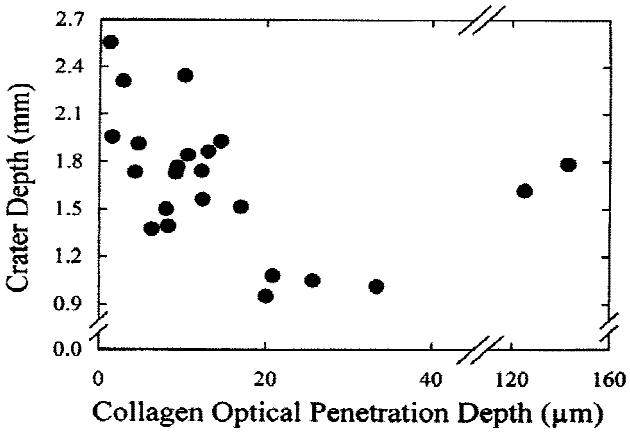

Fig. 7. Cut depth (millimeters) vs. optical penetration depth of collagen (micrometers) at the corresponding wavelength used to ablate cortical bone. With the exception of the two outlying data points generated by the 4.2- and 5.0-μm wavelengths, larger cut depths are achieved with radiation that is absorbed well by collagen.

There is no strong correlation between the

zone of collateral thermal injury and the optical absorption characteristics of the principle components of bone in the specimens of this study. As demonstrated in Table l, both wide and narrow zones of thermal injury are observed at wavelengths for which water or collagen have weak or strong absorption. Similarly, there is no correlation between optical absorption of the mineral component of bone and the observed collateral thermal injury.

The wide variability in the amount of thermal injury observed with the bone saw was attributed to heat generated by friction during the cut, and retention of heat in the saw blade between cuts. When using a bone saw, the generation of heat and the need for continual cooling at the surgical site are major concerns for orthopedic surgeons, and it seems that these problems may be reduced or eliminated by use of a laser for ablation.

Although a zone of empty lacunae adjacent to the ablation crater has been reported previously for bone ablations by using the FEL at 3.0, 6.1, and 6.45 μm [26], this was not observed in the specimens of this study. Although there may be some decrease in the total number of lacunae that contain cells adjacent to the ablation site, populated lacunae are present, and the distribution of populated and unpopulated lacunae appear to be no different than that observed for the bone saw cut specimens.

The observation of char on limited areas of some specimens at some wavelengths, but not uniformly on the walls of cuts, suggests that this char may not be a primary surface event, but the deposition of superheated debris from the plume back onto portions of the ablation surface. Wavelengths that produced deep cuts with minimal collateral thermal injury without evidence of char would be the most appropriate to select for further study.

It is likely that the surface characteristics observed on SEM examination at the base of the cut are most representative of the effects of the ablation event. With the equivalent of 30 macropulses per spot, the surface changes observed along the upper portion of the wall of the cut are likely manifestations of both the ablation process and the thermal and mechanical events resulting from the repeated passage of hot ablation plumes. This would explain the lack of correlation between the width of the zone of collateral thermal injury and the optical properties of bone and would be consistent with observations on collateral thermal injury reported for soft tissue [45].

Where crystals were observed on SEM examination, they were found on the upper third of the ablation crater wall or on the crater lip. The observed crystals are 2–3 orders of magnitude larger than the apatite crystals associated with bone. These observations suggest that the crystals were produced after superheating and subsequent cooling and were deposited or formed on the wall relative to passage of the ablation plume.

The SEM evaluation of the surface of the laser cut specimens shows characteristics distinctly different from the bone saw cuts, and these findings can be attributed to differences in the mechanisms of cutting bone in each case. The laser cuts are uniformly suggestive of an explosive event, where tissue has been ejected from the ablation surface. The bone saw cuts, with slabs and multiple microfissures, are most typical of mechanical shearing and suggests a less-stable postsurgical surface.

Previous investigations of laser bone ablation have reported a reduction of ablation efficiency with increasing pulse intensity at an energy density where a bright flash is observed emanating from the ablation site. Although the constituents of this flash and the mechanism of its production have been debated, its presence does appear to attenuate the influence of successive laser pulses directed at the same spot [6,15,19, 46–48]. To minimize the chances of pulse attenuation, a pulse intensity was selected below the threshold for induction of an observable flash, and the computer controlled delivery system was used to direct each successive macropulse to a different segment of the ablation line.

Before the initiation of this study, we determined that the threshold for the induction of a flash at the ablation site of rabbit cortical bone for wavelengths 3.0, 6.1, and 6.45 μm was 96 J/cm^2 (30 mJ/pulse, 200 μm spot diameter). To obtain comparative ablations for this study, we selected a single pulse intensity for use with all wavelengths. We chose the incident energy density of 72 J/cm^2 (22.5 ± 2.5 mJ/pulse, 200 μm spot diameter) which would be well above the expected ablation threshold to achieve maximal ablation for each wavelength, but would avoid any interference with ablation efficiency which might be experienced at higher energy densities.

Numerous studies of hard tissue (enamel,

dentin, and/or bone) ablation by using near to mid-IR wavelengths have been reported [1–26, 46–50]. These studies have demonstrated that hard tissue can be ablated by using near to mid-IR wavelengths with adjacent thermal damage limited to 10–20 μm when pulse durations between 0.1 and 200 μs are used. The influence of pulse durations in the ns, μs, and ms domains on the ablation of hard tissue have been investigated for several wavelengths in the near to mid-IR region, with the observation that ablation efficiency is best achieved with pulse durations between 0.1 and 200 μs [5,6,46–48].

Wavelength dependence of hard tissue ablations has been studied by comparison of ablations within limited regions of the IR spectrum, including 2.1–2.94 μm [16,25], 6.0–7.5 μm [49], and 9.6–10.6 μm [5,6,46,47]. Some studies have compared ablations made with wavelengths which are absorbed by different constituents of hard tissue. With one exception, these studies are limited to comparisons of erbium laser systems, where water is a primary absorber of the wavelength generated, and CO_2 laser systems where mineral absorption predominates [12,24,48]. Although one study makes a case for wavelength independence in dentin [49], all of the reported studies do demonstrate some differences between wavelengths in hard tissue, and the body of information suggests that wavelength dependence of ablation efficiency should be expected.

The study reported here is the first to compare ablations across the near to mid-IR region by using the same pulse structure and intensity, with the intensity well above the ablation threshold and a beam delivery procedure that minimizes optical attenuation of successive macropulses. Our observations are consistent with previous conclusions that the ablation mechanism below plasma threshold at these macropulse durations is due to an explosive event resulting from water vaporization in a confined space [6,15,18,24]. However, this study also demonstrates that the ablation of bone is enhanced by targeted weakening of the protein matrix, which provides the mechanical confinement that must be overcome by the expanding vapor pressure to achieve material removal.

This study confirms that ablation of cortical bone can be obtained with minimal collateral thermal injury across the near to mid-IR spectrum; demonstrates that the cut depth correlates most strongly with the absorption properties of collagen; and cut depth is least deep where the absorption properties of the mineral component of bone predominate. The ability to produce a 300–400-μm-wide, 3.0-mm-deep, 6.6-mm-long ablation in 33 seconds with less than 10 μm of collateral thermal injury and no charring, indicates that use of wavelengths in the 6.1 amide I to 6.45 μm amide II region, with the pulse characteristics described, should be useful for efficient cutting of cortical bone. Characterization and comparison of bone ablations by using 6.1 and 6.45 μm with this pulse structure in an in vivo model followed by healing studies are warranted.

ACKNOWLEDGMENTS

The authors thank Amy Nunnally of the W. M. Keck Free-Electron Laser Center, Vanderbilt University, and Lih-Hue L. Liaw, Angela Liogys, and Leslie Sabiniano of the Beckman Laser Institute and Medical Clinic, University of California, Irvine, for their technical assistance with this project. Special thanks to Paulette Spencer D.D.S., Ph.D., School of Dentistry, University of Missouri-Kansas City, for her review, suggestions, and encouragement during the preparation of this manuscript.

REFERENCES

1. Biyikli S, Modest MF. Energy requirements for osteotomy of femora and tibiae with a moving CW CO_2 laser. Lasers Surg Med 1987;7:512–519.
2. Clauser C. Comparison of depth profile of osteotomies performed by rapid superpulsed and continuous wave CO_2 laser beams at high power output. J Oral Maxillofac Surg 1986;44:425–430.
3. Clayman L, Fuller T, Beckman H. Healing of continuous-wave and rapid superpulsed carbon dioxide laser-induced bone defects. J Oral Maxillofac Surg 1978;36:932–937.
4. Clayman L. Bone response to carbon-dioxide, rapid-super-pulse, and continuous wave laser osteotomy in albino rabbits. Bull Sinai Hosp Detroit 1976;24:189.
5. Ertl T, Muller G. Hard tissue ablation with pulsed CO_2 lasers. San Jose: SPIE Biomedical Optics; 1993.
6. Forrer M, Frenz M, Romano V, et al. Bone-ablation mechanism using CO_2 lasers of different pulse duration and wavelength. Appl Phys B 1993;56:104–112.
7. Gertzbein SD, de Demetro D, Cruickshank B. The effect of laser osteotomy on bone healing. Lasers Surg Med 1981;1:361–373.
8. Gonzalez C, Van De Merwe WP, Smith M, Reinisch L. Comparison of the erbium yttrium aluminum garnet and

carbon dioxide lasers for in vitro bone and cartilage ablation. Laryngoscope 1990;100:13–17.
9. Izatt JA, Sankey ND, Parovi F, et al. Ablation of calcified biological tissue using pulsed hydrogen fluoride laser radiation. IEEE J Quant Elect 1990;26:2261–2270.
10. Kitai MS, Sobol EN, Sviridov AP, Omel'chenko AI. Manifestations of photochemical reactions in bone tissue on exposure to the ultraviolet radiation of an Eximer laser. Biophysics 1996;41:1151–1157.
11. Krause LS, Cobb CM, Rapley JW, Killoy WJ, Spencer P. Laser irradiation of bone: I. An in vitro study concerning the effects of the CO_2 laser on oral mucosa and subjacent cortical bone. J Periodontol 1997;68:872–880.
12. Li Z-Z, Reinisch L, Van de Merwe WP. Bone ablation with Er:YAG and CO_2 laser: study of thermal and acoustic effects. Lasers Surg Med 1992;12:79–85.
13. Nelson JS, Yow L, Liaw LH, et al. Ablation of bone and methacrylate by a prototype mid-infrared Erbium:YAG laser. Lasers Surg Med 1988;8:494–500.
14. Nelson JS, Orenstein A, Liaw LH, Berns MW. Mid-infrared Erbium:YAG laser ablation of bone: the effect of laser osteotomy on bone healing. Lasers Surg Med 1989; 9:362–374.
15. Nuss RC, Fabian RL, Sarker R, Puliafito CA. Infrared laser bone ablation. Lasers Surg Med 1988;8:381–391.
16. Romano V, Rodriguez R, Altermatt HJ, Frenz J, Weber HP. Bone microsurgery with IR-laser: a comparative study of the thermal action at different wavelengths. San Jose: SPIE Biomedical Optics; 1994.
17. Small IA, Osborn TP, Fuller T, Hussain M, Kobernick S. Observations of carbon dioxide laser and bone burr in the osteotomy of the rabbit tibia. J Oral Maxillofac Surg 1979;37:159–166.
18. Walsh JT, Flotte TJ, Deutsch TF. Er:YAG laser ablation of tissue: effect of pulse duration and tissue type on thermal damage. Lasers Surg Med 1989;9:314–326.
19. Walsh JT, Deutsch TF. Er:YAG laser ablation of tissue: measurement of ablation rates. Lasers Surg Med 1989;9: 327–337.
20. Walsh JT, Deutsch TF. Pulsed CO_2 laser ablation of tissue: measurement and modeling of ablation rates. IEEE Trans Biomed Eng 1989;36:1195–1201.
21. Walsh JT, Deutsch TF. Measurement of Er:YAG laser ablation plume dynamics. Appl Phys B 1991;52:217–224.
22. Wong B, Sung V, Berns MW, Svaasand LO, Neev J. Holmium-YAG laser ablation characteristics in calvarial lamellar and cortical bone: the role of water and tissue micro-architecture. Lasers Med Sci 1995;10:181–188.
23. Nelson JS, Orenstein A, Liaw LH, Zavar RB, Gianchandani S, Berns MW. Ultraviolet 308-nm excimer laser ablation of bone: an acute and chronic study. Appl Optics 1989;28:2350–2357.
24. Fried D, Zuerlein M, Featherstone JDB, Seka W, Duhn C, McCormack SM. IR laser ablation of dental enamel: mechanistic dependence on the primary absorber. Appl Surf Sci 1998;129:852–856.
25. Alshuler GB, Belikov AV, Erofeev AV. Laser treatment of enamel and dentine by different Er-lasers. Los Angeles: SPIE Biomedical Optics; 1994.
26. Spencer P, Payne JT, Cobb CM, et al. Effective laser ablation of bone based on the absorption characteristics of water and protein. J Periodontol 1999;70:68–74.
27. Reinisch L, Mendenhall M, Charous S, Ossoff RH. Computer-assisted surgical techniques using the Vanderbilt free electron laser. Laryngoscope 1994;104:1323–1329.
28. Skinner HCW. Bone: cellular and molecular organization. In: Albright J, Brand R, editors. Bone: cellular and molecular organization. New York: Appleton-Century-Crofts; 1979. p 105–134.
29. Neuman WF, Neuman MW. The chemical dynamics of bone mineral. Chicago: The University of Chicago Press; 1958.
30. Albright JA. Bone: Physical properties. In: Albright JA, Brand RA, editors. The scientific basis of orthopedics. New York: Appleton-Century-Crofts; 1979. p 135–183.
31. Jee WS. The skeletal tissues. In: Weiss L, editor. Cell and tissue biology. Baltimore and Munich: Urband and Schwarzenberg; 1988. p 211–254.
32. Rossert J, de Crombrugghe B. Type I collagen: structure, synthesis, and regulation. In: Bilezikian JP, Raisz LG, Rodan GA, editors. Principles of bone biology. San Diego: Academic Press; 1996. p 3–14.
33. Posner A, Betts F, Blumenthal N. Formation and structure of synthetic and bone hydroxyapatite. Prog Crystal Growth Charact 1980;3:49–64.
34. Posner A. Bone mineral and mineralization process. In: Peck W, editor. Bone and mineral research. New York: Elsevier; 1987. p 65–116.
35. Hale GM, Querry MR. Optical constants of water in the 200-nm to 200-um wavelength region. Applied Optics 1973;12:555–563.
36. Doyle BB, Bendit EG, Blout ER. Infrared spectroscopy of collagen and collagen-like polypeptides. Biophysics 1975; 14:937–957.
37. Yannas IV. Collagen and gelatin in the solid state. J Macromol Sci - Revs Macromol Chem 1972;C7:49–104.
38. Rey C, Shimizu M, Collins B, Glimcher MJ. Resolution-enhanced Fourier transform infrared spectroscopy study of the environment of phosphate ions in early deposits of a solid phase calcium phosphate in bone and enamel and their evolution with age. I: investigations in the v4 PO4 domain. Calcif Tissue Int 1990;46:384–394.
39. Rey C, Shimizu M, Collins B, Glimcher MJ. Resolution-enhanced Fourier transform infrared spectroscopy study of the environment of phosphate ions in early deposits of a solid phase calcium phosphate in bone and enamel and their evolution with age. II: Investigations in the v3 PO4 domain. Calcif Tissue Int 1991;49:383–388.
40. Paschalis EP, DiCarlo E, Betts F, Sherman P, Mendelsohn R, Boskey AL. FTIR microspectroscopic analysis of human osteonal bone. Calcif Tissue Int 1996;59:480–487.
41. Miller FA, Wilkins CH. Infrared spectra and characteristic frequencies of inorganic ions. Anal Chem 1952;24: 1253–1254.
42. Fowler BO. Infrared studies of apatites. I. Vibrational assignments for calcium, strontium, and barium hydroxyapatites utilizing isotopic substitution. Inorg Chem 1974;13:194–207.
43. Edwards G, Logan R, Copeland M, et al. Tissue ablation by a free-electron laser tuned to the amide II band. Nature 1994;371:416–419.
44. Payne BP, Nishioka NS, Mikic BB, Venugopalan V. Comparison of pulsed CO_2 laser ablation at 10.6 μm and 9.5 μm. Lasers Surg Med 1998;23:1–6.
45. Zweig AD, Meierhofer B, Muller OM, et al. Lateral ther-

mal damage along pulsed laser incision. Lasers Surg Med 1990;10:262–274.
46. Krapchev VB, Rabii CD, Harrington JA. Novel CO_2 system for hard tissue ablation. Los Angeles: SPIE Biomedical Optics; 1994.
47. Fried D, Murray MW, Featherstone JDB, et al. Dental hard tissue modification and removal using sealed TEA lasers operating at 9.6 μm and 10.6 μm. San Jose: SPIE Biomedical Optics; 1999.
48. Lukac M, Hocevar F, Simona C, et al. Effects of pulsed CO_2 and Er:YAG lasers on enamel and dentin. Los Angeles: SPIE Biomedical Optics; 1993.
49. Ostertag M, McKinley JT, Reinisch L, Harris DM, Tolk NH. Laser ablation as a function of the primary absorber in dentin. Laser Surg Med 1997;21:384–394.
50. Fried D, Borzillary SF, McCormack SM, Glena RE, Featherstone JDB, Seka W. The thermal effects on CO_2 laser irradiated dental enamel at 9.3, 9.6, 10.3, and 10.6 um. Laser Surgery Advanced Characterization, Therapeutics, and Systems IV, 1994.